JACS
JOURNAL OF THE AMERICAN CHEMICAL SOCIETY
Article
pubs.acs.org/JACS

Heterogeneous Electron Transfer from Dye-Sensitized Nanocrystalline TiO_2 to $[Co(bpy)_3]^{3+}$: Insights Gained from Impedance Spectroscopy

Yeru Liu,[†,‡] James R. Jennings,[†,‡] Shaik M. Zakeeruddin,[§] Michael Grätzel,[§] and Qing Wang*[,†]

[†]Department of Materials Science and Engineering, Faculty of Engineering, NUSNNI-NanoCore, National University of Singapore, Singapore 117576

[§]Laboratory of Photonics and Interfaces, Institute of Chemical Science and Engineering, Faculty of Basic Science, École Polytechnique Fédérale de Lausanne, CH-1015 Lausanne, Switzerland

Supporting Information

ABSTRACT: Dye-sensitized solar cells (DSCs) employing the $[Co(bpy)_3]^{3+/2+}$ redox mediator have recently attained efficiencies in excess of 12%, increasing the attractiveness of DSCs as an alternative to conventional photovoltaics. Heterogeneous electron transfer from dye-sensitized nanocrystalline TiO_2 to $[Co(bpy)_3]^{3+}$ ions in solution, a process known as recombination in the context of DSC operation, is an important loss mechanism in these solar cells. Here, we employ impedance spectroscopy over a range of temperatures to characterize electron storage, transport, and recombination in efficient DSCs based on the $[Co(bpy)_3]^{3+/2+}$ redox mediator, with either the amphiphillic ruthenium sensitizer Z907 or the state-of-the-art organic sensitizer Y123. The temperature dependence of the electron-transport resistance indicates that transport occurs via states at energies lower than commonly assumed for the TiO_2 conduction band edge. We show that a non-exponential dependence of capacitance, transport resistance, and recombination resistance on photovoltage can be interpreted as evidence for partial unpinning of the TiO_2 energy levels. We also find that the nature of the sensitizing dye determines the predominant recombination route: via the conduction band for Y123 and via band gap states for Z907, which is the main reason for the superior performance of Y123. The different mechanisms appear to arise from changes in electronic coupling between TiO_2 donor states and $[Co(bpy)_3]^{3+}$ acceptor states, as opposed to changes in the density of TiO_2 states or their energetic matching with the acceptor-state distribution. These findings have implications for modeling heterogeneous electron transfer at dye-sensitized semiconductor−solution interfaces in general and for the optimization of DSCs.

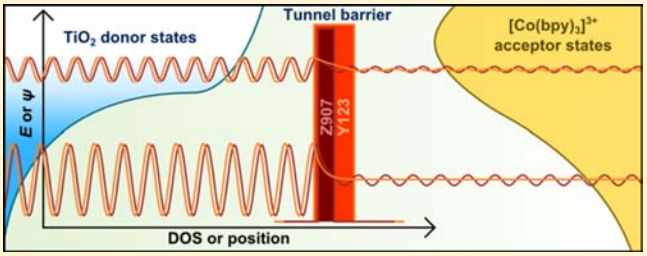

1. INTRODUCTION

Power conversion efficiencies (PCEs) in excess of 12% have recently been achieved for dye-sensitized solar cells (DSCs),[1−3] increasing their attractiveness as an alternative to conventional photovoltaics. The basic components of a DSC are a photoanode, a cathode, and an electrolyte solution containing a redox couple. The photoanode is almost always a porous nanocrystalline TiO_2 layer coated with a monolayer of chemisorbed dye molecules, supported on a conductive SnO_2:F substrate. The photoanode is separated from the cathode (which usually consists of SnO_2:F coated with a thin layer of Pt) by a ∼20 μm thick gasket made of a hot-melt polymer. The redox electrolyte solution fills the space between the electrodes and penetrates the pores of the TiO_2 layer, intimately contacting the dye monolayer. In operation, dye molecules are excited by absorption of incident photons, resulting in rapid electron injection into the TiO_2.[4] Following injection, the now oxidized dye is reduced back to its original state by an electron donor in the redox electrolyte (a process known as regeneration), enabling it to undergo another round of excitation and injection.[5] Meanwhile, injected electrons are transported to the SnO_2:F substrate by a multiple-trapping or hopping mechanism[6,7] where they flow into the external circuit and do potentially useful work when passing through a load, before reaching the cathode where they expend the remainder of their potential energy to re-reduce redox species that were oxidized in the dye regeneration process.

The most commonly employed redox couple in DSCs is I_3^-/I^-,[8] although several other very promising alternatives have been investigated.[9−13] The $[Co(bpy)_3]^{3+/2+}$ couple in particular has recently achieved success on par with I_3^-/I^-.[2] Nusbaumer and co-workers reported the first detailed investigation into the use of a cobalt complex as a redox mediator in DSCs.[14] Several other groups then evaluated similar complexes and further investigated factors limiting device efficiency.[15−24] It was generally agreed that complexes bearing bulky substituents were required to inhibit recombination at the semiconductor−

Received: December 2, 2012
Published: February 20, 2013

 © 2013 American Chemical Society dx.doi.org/10.1021/ja311743m | J. Am. Chem. Soc. 2013, 135, 3939−3952

solution interface, but that this also led to lower diffusion coefficients and consequently to mass-transport limitation of photocurrent and fill factor (FF). The first in a series of breakthroughs in performance under full solar light came when Feldt and co-workers found that, by adding bulky substituents to a high-extinction-coefficient organic dye, they were able to slow recombination enough to use the relatively small $[Co(bpy)_3]^{3+/2+}$ mediator.[10] This mediator does not suffer so much from mass-transport problems, leading to higher photocurrent and FF, and has a more suitable redox potential than bulkier cobalt complexes, leading to higher photovoltage. Following this report, Tsao and co-workers reported an efficiency of 9.6% using a newly synthesized cyclopentadithiophene-bridged donor−acceptor dye named Y123,[25] before Yella and co-workers attained the current record efficiency by co-sensitizing the TiO_2 with Y123 and a novel porphyrin dye.[2]

To further improve the efficiency of DSCs based on the $[Co(bpy)_3]^{3+/2+}$ mediator, improvements in several areas will be required. For example, to achieve higher photocurrents it will be necessary to develop new dye molecules that can harvest energy from the abundant but under-utilized near-infrared photons present in sunlight. At the same time, free energy losses required for efficient charge separation and mass transport through the cell must be minimized in order to maximize photovoltage and achieve good FFs. Equally or possibly more important is the need to understand and reduce unwanted recombination, which will ultimately limit photovoltage, FF, and efficiency once other aspects of the solar cell are fully optimized. The recombination process in efficient $[Co(bpy)_3]^{3+/2+}$-based DSCs is heterogeneous electron transfer from the dye-sensitized TiO_2 electrode to $Co[(bpy)_3]^{3+}$ ions in solution, and elucidating the details of this critical process in functional DSCs was a major objective of the present work.

Most previously published studies of recombination in DSCs employing cobalt-based mediators utilized the ruthenium-based sensitizers known as N3 and N719. Here, we focus on DSCs employing the state-of-the-art organic sensitizing dye Y123, so that comparatively high overall PCEs are achieved. We also study DSCs employing the ruthenium complex Z907 as sensitizer, in order to elucidate the reason for the lower photovoltage, FF, and PCE compared to Y123. We use impedance spectroscopy (IS) to characterize electron storage, transport, and recombination over a range of different temperatures, in addition to the more typical variation of incident light intensity and cell voltage. The additional independent variable enables us to obtain important information about charge carrier transport and system energetics, which are needed to properly understand and model recombination. We use the temperature and voltage dependence of the TiO_2 capacitance and electron-transport resistance to determine an effective electron-transport energy, which is found to be much lower than common estimates for the TiO_2 conduction band edge. We also find a non-exponential dependence of TiO_2 capacitance and transport resistance on cell voltage, which may imply that a partial unpinning of the TiO_2 energy levels occurs for both sensitizers. We go on to show how this effect can be properly accounted for when modeling recombination, before comparing various different recombination schemes, with and without the assumption of pinned TiO_2 energy levels. For the Y123 sensitizer, we find that recombination cannot be adequately modeled using any reasonable electron-transfer scheme if it is assumed that the TiO_2 energy levels are pinned. If unpinning of energy levels is allowed, a model in which recombination occurs via the conduction band can explain our data, provided that the rate constant for electron transfer depends upon the electric potential difference across the TiO_2−solution interface according to simple Butler−Volmer kinetics. In contrast, recombination via band gap states is needed to adequately model the data for Z907, regardless of whether the TiO_2 energy levels are assumed to be unpinned. The different recombination mechanisms seem to arise due to changes in electronic coupling between TiO_2 donor states and $[Co(bpy)_3]^{3+}$ acceptor states, as opposed to a change in the density of TiO_2 states or their energetic matching with the acceptor-state distribution, as evidenced by capacitance data, transport data, and extensive simulations of recombination. The difference in predominant recombination pathways is a major reason for the difference in efficiency between the two dyes and has implications for the optimization of DSCs, as well as for the modeling of heterogeneous electron transfer at dye-sensitized semiconductor−solution interfaces in general.

2. EXPERIMENTAL SECTION

2.1. Fabrication of Dye-Sensitized Solar Cells. The DSC fabrication procedure used in this work has been described in detail elsewhere.[26] In brief, 5 μm thick nanocrystalline TiO_2 layers were prepared by screen-printing a commercially available TiO_2 paste (Dyesol 18NR-T) onto FTO substrates that had previously been coated with compact TiO_2 blocking layers using spray pyrolysis.[27] The sensitizing dye was either 3-(6-(4-[bis(2′,4′-dihexyloxybiphenyl-4-yl)amino]phenyl)-4,4-dihexylcyclopenta-[2,1-*b*:3,4-*b*′]dithiphene-2-yl)-2-cyanoacrylic acid (Y123)[25] or *cis*-diisothiocyanato-(2,2′-bipyridyl-4,4′-dicarboxylic acid)-(2,2′-bipyridyl-4,4′-dinonyl)ruthenium(II) (Z907, Dyesol), and the electrolyte consisted of either 0.2 M $[Co(bpy)_3](PF_6)_2$ (synthesized as reported previously),[28] 0.02 M $[Co(bpy)_3](PF_6)_2BF_4$ (produced by oxidation of $[Co(bpy)_3](PF_6)_2$ using $NOBF_4$), 0.1 M $LiClO_4$, and 0.5 M 4-*tert*-butylpyridine in acetonitrile (coded as "Co" electrolyte) or 0.6 M PMII, 0.03 M I_2, 0.1 M guanidinium thiocyanate, and 0.5 M 4-*tert*-butylpyridine in an 85:15 (v/v) mixture of acetonitrile and valeronitrile (coded as "I" electrolyte). The counter electrode was made from a piece of platinized FTO, and the cell was sealed using a hot-melt polymer (Meltonix 1170-25, Solaronix). The active area of the DSCs was 0.28 cm^2.

2.2. Impedance Spectroscopy Measurements. IS measurements were made using an Autolab potentiostat/galvanostat (PGSTAT 302N, Ecochemie) equipped with a frequency response analyzer and controlled by the Nova 1.6 software package. The frequency range was 0.1 Hz−100 kHz, and the measuring perturbation was 15 mV RMS. Measurements were performed while cells were under illumination by red light (center wavelength 627 nm) provided by a light-emitting diode (Luxeon Rebel Tri-Star), and cells were biased to the open-circuit photovoltage produced by the illumination. To achieve a range of photovoltages, the light intensity was varied using neutral density filters mounted in a computer-controlled motorized filter wheel. The optical density of the filters was varied in steps of 0.5, and the highest light intensity used was sufficient to produce a photovoltage similar to that obtained under simulated 100 mW cm^{-2} AM1.5G illumination. To control the temperature of cells during the measurements, they were mounted on a Peltier element using a thin layer of thermally conductive heatsink compound. The temperature was monitored using a thermocouple mounted on the cells.

2.3. Electrochemical Measurements. Redox Fermi energies of the solar cell electrolytes were measured relative to a Ag/Ag^+ non-aqueous reference electrode (Ag|0.01 M $AgNO_3$, 0.1 M TBAP in acetonitrile) by potentiometry using a Pt wire. The measurements were performed in a non-isothermal cell consisting of two main compartments separated by a Teflon tube, all of which were filled with

a 0.1 M TBAP solution in acetonitrile. Each compartment was immersed in a water bath to facilitate temperature control. One compartment was maintained at approximately room temperature while the temperature of the other compartment was varied. Smaller compartments containing reference electrodes or solar cell electrolyte samples were placed into the main compartments, separated from them using porous Vycor frits.

3. RESULTS AND DISCUSSION

3.1. Temperature Dependence of TiO_2 Density of States and Electrolyte Redox Fermi Energy. IS measurements were performed over a range of temperatures and photovoltages (V_{oc}) on DSCs employing I_3^-/I^- as redox mediator and Z907 as sensitizer (cells referred to as Z907-I) or $[Co(bpy)_3]^{3+/2+}$ as redox mediator and either Z907 or Y123 as sensitizer (cells referred to as Z907-Co or Y123-Co); current−voltage characteristics of these cells are shown in Figure S1 in the Supporting Information. Impedance spectra were analyzed using a well-known equivalent circuit[29] (Figure S2) to obtain the capacitance (C_{meas}), electron-transport resistance (R_t), and recombination resistance (R_{rec}) of the TiO_2 layer. Figure 1a−c shows the dependence of C_{meas} on V_{oc} at temperatures ranging from 280 to 328 K for Z907-I, Z907-Co, and Y123-Co.

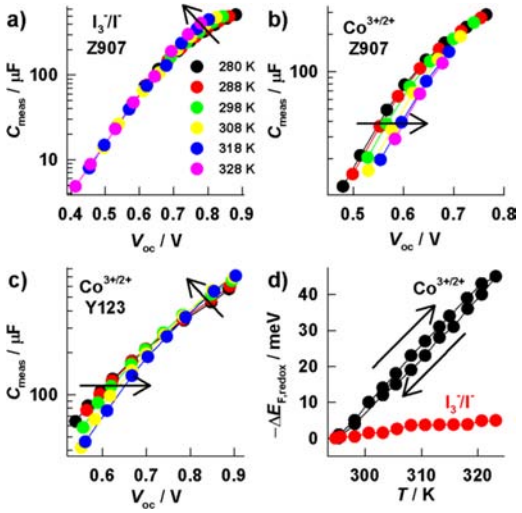

Figure 1. Temperature dependence of capacitance−photovoltage (C_{meas}−V_{oc}) characteristics for DSCs employing I_3^-/I^- as redox mediator and Z907 as sensitizer (a) or $[Co(bpy)_3]^{3+/2+}$ as redox mediator and either Z907 (b) or Y123 (c) as sensitizer. Changes in the electrolyte redox Fermi energy relative to 295 K ($\Delta E_{F,redox}$) as a function of temperature are also shown (d). The arrows in a−c indicate increasing temperature, while the arrows in d indicate the direction of the temperature sweep.

The main contribution to C_{meas} is believed to be a chemical capacitance associated with trap states that can be approximated as[30]

$$C_{meas} \approx LA(1-p)q^2 g({}_nE_F) \quad (1)$$

where L is the TiO_2 layer thickness, A is the area, p is the porosity, q is the elementary charge, and $g({}_nE_F)$ is the TiO_2 density of states (DOS) at the electron quasi-Fermi energy (${}_nE_F$). Under open-circuit conditions ${}_nE_F$ is related to V_{oc} by

$$qV_{oc} = {}_nE_F - E_{F,redox} \quad (2)$$

where $E_{F,redox}$ is the redox Fermi energy of the electrolyte. Wherever eq 1 is valid, C_{meas}−V_{oc} plots can be considered to directly reveal the TiO_2 DOS function, $g(E)$. As reported previously for a very similar I_3^-/I^- electrolyte,[31] semi-log C_{meas}−V_{oc} plots for Z907-I are linear and almost independent of temperature for voltages below ∼0.65 V. It follows from eqs 1 and 2 that this can be interpreted as evidence for an exponential distribution of band gap trap states with a DOS function that can be expressed as

$$g_t(E) = \frac{N_t}{k_B T_c} \exp\left(\frac{E - E_c}{k_B T_c}\right) \quad (3)$$

where N_t is the density of trap states at the conduction band edge, k_B is Boltzmann's constant, T_c is a characteristic temperature related to the curvature of the trap distribution, and E_c is the energy of the conduction band edge. The slope of the semi-log C_{meas}−V_{oc} plots in Figure 1a yields T_c = 860 K for Z907-I below ∼0.65 V where the plots are linear, which is close to previously reported values.[31] The deviation from linearity above ∼0.65 V, which is not predicted by eqs 1−3, will be discussed shortly.

The C_{meas}−V_{oc} plots for both cells employing the $[Co(bpy)_3]^{3+/2+}$ electrolyte are markedly different from those for the I_3^-/I^- electrolyte. The plots for Z907-Co are approximately parallel at low V_{oc} with $T_c \approx 720$ K; however, in contrast to Z907-I, the plots shift along the V_{oc} axis toward higher V_{oc} with increasing temperature. Plots for Y123-Co are not parallel at any V_{oc}, with T_c values (estimated at low V_{oc}) decreasing from 1350 to 1140 K as temperature increases from 280 to 320 K. Shifts toward higher V_{oc} with increasing temperature could also explain some of the trends in the Y123-Co data, but this interpretation is complicated by the temperature-dependent slopes. As shown by eqs 1−3, a likely explanation for the shifts between the C_{meas}−V_{oc} plots is that one or more of N_t, E_c, or $E_{F,redox}$ is temperature-dependent. To help establish the main cause, we have measured $E_{F,redox}$ as a function of temperature using a non-isothermal cell. To do this we assume that negligible Soret and Thompson potentials exist in our cell[32] and also that negligible changes in isothermal liquid junction potentials occur when the temperature is changed. Significant isothermal liquid junction potentials probably *do* exist in this experiment, but provided that they are approximately constant over the studied temperature range, the change in redox Fermi energy, $\Delta E_{F,redox}$, can still be estimated.

Figure 1d shows how $\Delta E_{F,redox}$ varies with temperature for both I_3^-/I^- and $[Co(bpy)_3]^{3+/2+}$ electrolyte solutions. Interestingly, the dependence of $\Delta E_{F,redox}$ on temperature for the $[Co(bpy)_3]^{3+/2+}$ electrolyte is of the correct sign (note that in this work $E_{F,redox}$ is defined as an electron energy, *not* a potential) and approximately the correct magnitude to cause the shifts between C_{meas}−V_{oc} plots. For the I_3^-/I^- electrolyte, the relative invariance of $\Delta E_{F,redox}$ with temperature is also fully consistent with the overlap between C_{meas}−V_{oc} plots over most of the voltage range. Taken together, the results shown in Figure 1 strongly suggest that the shifts in C_{meas}−V_{oc} plots for the $[Co(bpy)_3]^{3+/2+}$ electrolyte are mainly caused by changes in $E_{F,redox}$. It is worth noting here that Gritzner and co-workers have observed a very similar temperature dependence for the polarographic half-wave potential of the $[Co(bpy)_3]^{3+/2+}$ couple in the same solvent: 2.22 mV K^{-1} versus our result of 1.62 meV K^{-1} for $-\Delta E_{F,redox}$.[33] The small discrepancy can probably be attributed to the fact that we measured $\Delta E_{F,redox}$ using

dx.doi.org/10.1021/ja311743m | J. Am. Chem. Soc. 2013, 135, 3939−3952

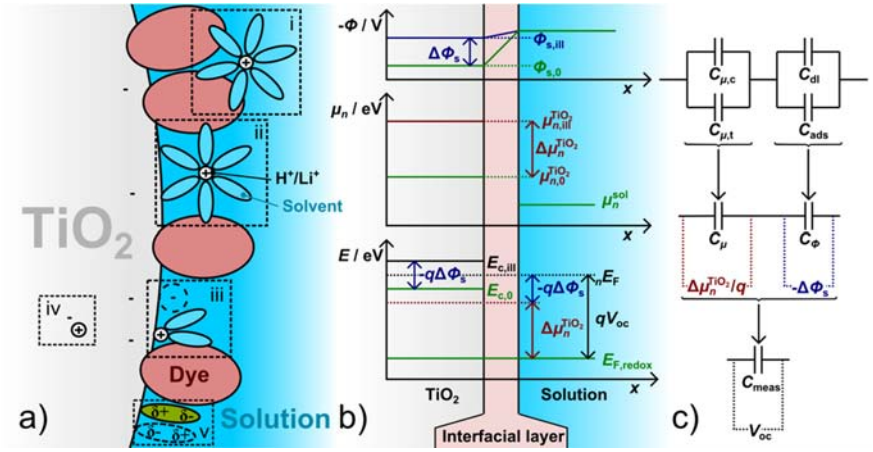

Figure 2. (a) Diagram illustrating possible locations of counter charge and changes in double-layer structure associated with injecting excess electronic charge into a dye-sensitized TiO_2 particle. Solvated cations may be separated from the surface of the TiO_2 by the dye monolayer (i), solvated cations may penetrate the dye layer (ii), the surface concentration of specifically adsorbed ions may be perturbed (iii), and small cations may be intercalated into the TiO_2 lattice (iv). Note that only excess charge is shown; charge present at equilibrium in the dark is not drawn. The change in the electric potential in the TiO_2, $\Delta\phi_s$, caused by the excess charge decreases from i to iv. It is also possible that the excess charge perturbs adsorption equilibria of solvent molecules and other polar electrolyte species (v), again leading to a change in ϕ_s. (b) Diagram illustrating the spatial distribution of electric potential (ϕ), electron chemical potential (μ_n), and total energy (E) under illumination/forward bias (denoted by subscript "ill") or in the dark (denoted by subscript "0") at a dye-sensitized TiO_2–solution interface. Electric fields in the TiO_2 particle are neglected, and it is assumed that there is a net field in the interfacial layer pointing away from the TiO_2 particle at equilibrium in the dark. (c) Equivalent circuit diagram for the TiO_2 capacitance showing the connectivity of the conduction band chemical capacitance ($C_{\mu,c}$), the band gap state chemical capacitance ($C_{\mu,t}$), the double-layer capacitance (C_{dl}), and the adsorption/intercalation capacitance (C_{ads}). Also indicated is how the circuit can be simplified to a single chemical capacitance (C_μ) connected in series with a single electrostatic capacitance ($C\phi$), and then further simplified to the single, measurable capacitance (C_{meas}).

potentiometry, not the half-wave potential, and that in our case a concentrated electrolyte with unequal concentrations of oxidized and reduced species was used.

Although an exponential distribution of trap states (eq 3) coupled with the temperature dependence of $E_{F,redox}$ can explain most of the C_{meas}–V_{oc} data in Figure 1, a few observations require further explanation. First, it is unclear why T_c depends upon the electrolyte composition, the dye molecule, and, for the Y123 dye, the temperature. Second, at sufficiently high V_{oc} all of the semi-log C_{meas}–V_{oc} plots are noticeably curved, which is not predicted by eq 3. If C_{meas} is still to be interpreted as a pure chemical capacitance, the associated electronic states must not be distributed exponentially. They must also be mostly located near the semiconductor–solution interface (there is some evidence for this in the literature),[34,35] so that their energetic distribution can be affected by interaction with the dye and species in solution. This is a plausible explanation and one that we cannot rule out. Another equally plausible interface-based explanation for these phenomena, with more precedence in the electrochemical literature, is that the semiconductor energy levels become partially unpinned, as will be elaborated on in the next section.[26,36,37]

3.2. Implications of Energy Level Unpinning for the Interpretation of C_{meas}–V_{oc} Data. Before discussing energy level unpinning further, it is necessary to clarify the meaning of this term in the context of DSCs and to define various related quantities. The basic concepts have already been covered by other authors,[38,39] but it is convenient to provide a summary here. We begin by noting that ${}_nE_F$ is equivalent to the electrochemical potential of electrons in the TiO_2, which can be written as

$$ {}_nE_F \equiv \bar{\mu}_n^{TiO_2} = \mu_n^{TiO_2} - q\phi_s \quad (4) $$

where $\mu_n^{TiO_2}$ and ϕ_s are the electron chemical potential and the electric potential in the TiO_2, respectively. For simplicity, we assume that both quantities are approximately independent of position in the TiO_2 layer and that there is negligible band bending in each individual TiO_2 particle.

When ${}_nE_F$ is displaced relative to $E_{F,redox}$ by a change in illumination intensity or applied bias, the TiO_2 energy levels are pinned if the entire variation in ${}_nE_F$ is caused only by a change in $\mu_n^{TiO_2}$. The energy levels are partially unpinned if significant changes in both $\mu_n^{TiO_2}$ and ϕ_s occur, and fully unpinned if only ϕ_s changes. In principle, some variation of ϕ_s must be expected when excess electronic charge is added to the TiO_2. The extent of this variation will depend upon the location of the positive counter charge, which may be in the electrolyte or intercalated into the TiO_2 lattice,[40] and upon whether the adsorption equilibria of various polar species (e.g., solvent molecules, *tert*-butylpyridine) are perturbed by the added charge. Several possible mechanisms of charge compensation are illustrated in Figure 2a. Figure 2b shows how the electric potential and the electron chemical potential vary on passing across the TiO_2–solution interface, at equilibrium in the dark and under illumination or applied bias, for the case of partially unpinned TiO_2 energy levels.

If the TiO_2 energy levels partially unpin, C_{meas} cannot be treated as a pure chemical capacitance. Provided that $E_{F,redox}$ remains constant, C_{meas} strictly corresponds to the *electrochemical* capacitance of the TiO_2 layer,[30]

$$ C_{meas} = C_{\bar{\mu}} = LA(1-p)q^2\frac{dn}{d_nE_F} \quad (5) $$

where n is the total electron density in the TiO_2. Equation 4 suggests that $C_{\bar{\mu}}$ can also be represented by a chemical capacitor,

dx.doi.org/10.1021/ja311743m | J. Am. Chem. Soc. 2013, 135, 3939–3952

$$C_\mu = LA(1-p)q^2\frac{dn}{d\mu_n^{TiO_2}} \quad (6)$$

in series with an electrostatic capacitor,

$$C_\phi = LA(1-p)q\frac{dn}{d\phi_s} \quad (7)$$

so that

$$\frac{1}{C_{\bar{\mu}}} = \frac{1}{C_\mu} + \frac{1}{C_\phi} \quad (8)$$

In the equivalent circuit analogy suggested above, C_μ can be considered to hold all of the excess negative charge in the TiO_2 on one of its plates. C_μ can be treated as the parallel combination of a trap state capacitance ($C_{\mu,t}$) and a conduction band capacitance ($C_{\mu,c}$).[30] For an exponential DOS given by eq 3, $C_{\mu,t}$ is related to V_{oc} by the approximate relation

$$C_{\mu,t} \approx LA(1-p)q^2\frac{N_t}{k_B T_c}\exp\left(\frac{qV_{oc} + E_{F,redox} - E_c + q\Delta\phi_s}{k_B T_c}\right) \quad (9)$$

where $\Delta\phi_s$ is the change in the electric potential in the TiO_2 relative to that at equilibrium in the dark. This term is needed if unpinning occurs because a change in ϕ_s causes a shift in E_c relative to $E_{F,redox}$ as indicated in Figure 2b. When ${}_nE_F$ is sufficiently below E_c, the functional form of $C_{\mu,c}$ is identical to that of eq 9, only with N_t replaced by the effective DOS at the conduction band edge (N_c) and with T_c replaced by the absolute temperature (T).

C_ϕ can be viewed as holding all of the excess positive charge in the system on one of its plates and may be treated as the parallel combination of a double-layer capacitance, C_{dl}, and a capacitance associated with specific adsorption (and possibly intercalation) of ions, C_{ads}. The value of C_{dl} (itself a serially connected Helmholtz capacitance and diffuse layer capacitance) depends on the distribution of counter charge in the electrolyte and in general may be potential-dependent. The value of C_{ads} is governed by potential-dependent adsorption isotherms for specifically adsorbed ions and possibly even intercalation isotherms for small cations like H^+ or Li^+. Here, we make no attempt to distinguish between these various contributions and from now on will simply refer to C_ϕ. The connectivity of the various chemical and electrostatic capacitors discussed above is indicated in Figure 2c.

If changes in $\Delta\phi_s$ under illumination are not negligible compared to V_{oc}, and therefore C_ϕ is not much larger than C_μ (i.e., if the TiO_2 energy levels partially unpin), semi-log C_{meas}–V_{oc} plots (e.g., Figure 1a–c) cannot be considered to directly reveal the TiO_2 band gap state DOS function and, therefore, are not expected to be linear, even if the DOS function is in fact exponential. It follows that if C_ϕ depends on the nature of the dye or the composition of the electrolyte solution, then the *apparent* TiO_2 band gap state DOS function, as inferred from C_{meas}–V_{oc} plots, will acquire a dye/electrolyte dependence, which may explain some of the above observations. However, observation of curved C_{meas}–V_{oc} plots cannot rule out the possibility that the TiO_2 DOS function is simply not exponential. In order to determine which explanation is more likely, it is important to examine the voltage dependence of the electron-transport resistance, R_t, as this is also expected to be sensitive to unpinning of the TiO_2 energy levels and, in certain cases, is insensitive to a non-exponential TiO_2 band gap state DOS function, as discussed below.

3.3. Estimation of the Electron-Transport Energy and Evidence for Energy Level Unpinning. For electron transport via a conduction band of extended electronic states, the TiO_2 electron-transport resistance can be written in terms of V_{oc} as

$$R_t = R_{t,0}\exp\left(-\frac{qV_{oc} + E_{F,redox} - E_c + q\Delta\phi_s}{k_B T}\right) \quad (10)$$

where $R_{t,0}$ is a constant related to the geometry of the TiO_2 film, the effective DOS at E_c, and the free electron mobility. The $\Delta\phi_s$ term is again needed to account for any possible unpinning of the TiO_2 energy levels. It is also worth noting that, in contrast to C_{meas}, measurement of R_t is unaffected by any partitioning of the applied AC potential between C_μ and C_ϕ because drift and diffusion are indistinguishable.[41] It is also possible to apply eq 10 to other transport mechanisms if E_c is defined as an effective transport energy and $R_{t,0}$ is appropriately redefined. Microscopic details of the transport mechanism are not necessarily needed, provided that (i) transport only occurs via states far above ${}_nE_F$ and (ii) electrons can be considered independently, which requires that electron–electron interactions are negligible. This follows from the Kubo–Greenwood transport formalism and applies for arbitrary DOS and an arbitrary energy dependence of the "mobility", which can be defined such that it accounts for the degree of localization or delocalization of the states involved in transport (Supporting Information).[42] The same conclusion can also be drawn for the specific case of hopping transport in an exponential DOS at low carrier density on the basis of the results of Monte Carlo simulations by Gonzalez-Vazquez and co-workers, where the concept of an effective transport energy is discussed in detail.[43]

Figure 3a,b shows semi-log R_t–V_{oc} plots for Z907-Co and Y123-Co at various temperatures. The plots appear to be quite

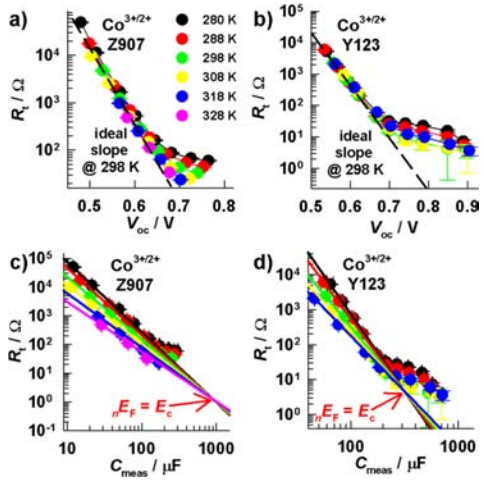

Figure 3. Dependence of TiO_2 electron-transport resistance (R_t) on photovoltage (V_{oc}) and temperature for DSCs employing $[Co(bpy)_3]^{3+/2+}$ as redox mediator and either Z907 (a) or Y123 (b) as sensitizer. The dashed lines indicate an ideal slope of 17 V^{-1} at 298 K. Also shown is the dependence of R_t on measured capacitance (C_{meas}) for the same DSCs (c,d). The intersection point of the extrapolated power law fit lines provides an estimate of the R_t and C_{meas} values that would be obtained if ${}_nE_F$ reached the transport energy.

dx.doi.org/10.1021/ja311743m | J. Am. Chem. Soc. 2013, 135, 3939–3952

weakly dependent on temperature compared to previous reports for the I_3^-/I^- redox mediator,[31] partly due to the temperature dependence of $E_{F,redox}$ which acts to shift the plots closer together. However, at low enough V_{oc} all plots do *approach* the "ideal" slope of $-q/(2.303k_BT)$ decades per V predicted by eq 10 when $\Delta\phi_s$ is zero (Supporting Information). As V_{oc} increases the plots curve and become progressively less ideal, a common phenomenon that has also been reported for the I_3^-/I^- mediator.[26] The simplest explanation for the near-ideal slope at low V_{oc} is that transport occurs via states far above ${}_nE_F$ and that the TiO_2 energy levels are pinned. However, the increasing non-ideality and curvature at higher V_{oc} demands a different explanation.

As mentioned above, several different transport mechanisms can in principle result in eq 10 being obeyed when ${}_nE_F$ is sufficiently below E_c. It is therefore reasonable to suggest that some of the "non-ideality" (i.e., deviation from eq 10 with zero $\Delta\phi_s$) found in the R_t–V_{oc} plots is caused by unpinning of the semiconductor energy levels. Another explanation for non-ideality is that transport occurs mostly via states that are not far above the ${}_nE_F$, so that eq 10 need not be obeyed. It is also possible that some combination of this together with partial energy level unpinning occurs. For example, at low V_{oc} non-ideality may be caused by a slight unpinning of the energy levels while at higher V_{oc}, ${}_nE_F$ may closely approach the states involved in transport. Equation 10 implies that measurements of R_t as a function of V_{oc} and temperature are sufficient to determine $E_c - E_{F,redox}$ if $\Delta\phi_s$ can be neglected. Knowledge of $E_c - E_{F,redox}$ would be useful as it would allow us to estimate how closely ${}_nE_F$ approaches E_c, thus providing information about the likely validity of eq 10. In previous works,[7,31] plots of R_t versus V_{oc} for different temperatures were extrapolated to find their intersection point and thus provide an estimate of $E_c - E_{F,redox}$. This approach is not possible here since we have shown that $E_{F,redox}$ in the $[Co(bpy)_3]^{3+/2+}$ system is a function of temperature and, unfortunately, we can only approximately quantify this due to unknown junction potentials. Furthermore, if the energy levels unpin then the $-q\Delta\phi_s$ term in eq 10 is not negligible. An alternative approach that mostly avoids these problems is to plot R_t versus C_{meas}, which in principle can be used as an accurate indicator of ${}_nE_F$ relative to E_c provided that $C_{meas} \approx C_{\mu,t}$.

It is easy to show from eqs 9 and 10 that the following relationship between R_t and $C_{\mu,t}$ should hold:

$$R_t = R_{t,0}\left(\frac{C_{\mu,t}}{C_{\mu,t,0}}\right)^{-1/\alpha} \tag{11}$$

where $R_{t,0}$ and $C_{\mu,t,0}$ are the values of R_t and $C_{\mu,t}$ predicted by eqs 9 and 10 for ${}_nE_F = E_c - q\Delta\phi_s$, and $\alpha = T/T_c$. From eq 11 it follows that double-logarithmic plots of R_t versus $C_{\mu,t}$ should have temperature-dependent slopes of $-1/\alpha$ and a common intersection point at $R_t = R_{t,0}$ and $C_{\mu,t} = C_{\mu,t,0}$. The value of $R_{t,0}$ can then be used in conjunction with R_t–V_{oc} data and eq 10 to estimate $E_c - q\Delta\phi_s - E_{F,redox}$ at any particular V_{oc}. Interestingly, the values of $R_{t,0}$ and $C_{\mu,t,0}$ obtained using this approach are completely insensitive to $E_{F,redox}$ and $\Delta\phi_s$ because these quantities appear in both eqs 9 and 10 so that they cancel when deriving eq 11. However, attenuation of C_{meas} due to the drop in AC voltage across C_ϕ (eq 8) does still affect the analysis by weakening the approximation $C_{meas} \approx C_{\mu,t}$. The analysis is also only strictly valid if $R_{t,0}$ and $C_{\mu,t,0}$ do not depend on temperature. For the case of conduction band transport this is likely to be the case (Figure S3). This is also likely to be approximately correct for hopping transport at sufficiently low carrier density.[7,43]

Figure 3c,d shows double-logarithmic plots of R_t versus C_{meas} at several different temperatures for Z907-Co and Y123-Co. The solid lines show global fits of eq 11 to the data for all temperatures. In these fits $1/\alpha$ was allowed to vary freely for each temperature, but the values of $R_{t,0}$ and $C_{\mu,t,0}$ were common to all temperatures to enforce a shared intersection point. Similar results can be obtained from completely free fits, but the intersection point is slightly less well-defined. In the interest of simplicity, we make the assumption that $R_{t,0}$ and $C_{\mu,t,0}$ are constants so that the best use of the available data is to perform a global fit. Only data where C_{meas} was less than ~100 μF were fitted to avoid the obvious deviation from linearity at higher C_{meas}. Importantly, this also excludes from the analysis all of the R_t data obtained at high V_{oc} where its validity might be questioned due to strongly overlapping time constants in the original impedance spectra.[21,24,44,45] Determination of $E_c - q\Delta\phi_s - E_{F,redox}$ using this approach can therefore be viewed as being quite robust in this respect.

T_c values (i.e., T/α) calculated from the fit for Z907-Co are approximately constant, which goes some way toward validating the analysis (Figure S10). From the intersection point of the fit lines, $R_{t,0}$ is found to be ~1.3 Ω, and it can be estimated that ${}_nE_F \approx 90$ meV below $E_c - q\Delta\phi_s$ for the lowest measured value of R_t at 298 K. This is just low enough to ensure that Boltzmann statistics hold for the occupancy of states at $E_c - q\Delta\phi_s$, and thus there is a good chance that eq 10 is valid. This adds weight to the argument that the non-ideality in R_t–V_{oc} characteristics is caused by the TiO_2 energy levels unpinning. The value of $E_c - q\Delta\phi_s - E_{F,redox}$ calculated for the lowest V_{oc} (highest R_t) is 0.74 eV, which presumably is close to $E_c - E_{F,redox}$ at equilibrium in the dark, where by definition $\Delta\phi_s = 0$. This estimate of $E_c - E_{F,redox}$ is very low compared with commonly assumed values,[46,47] suggesting that electron transport may not occur solely via the conduction band and that $E_c - E_{F,redox}$ may be better interpreted as an effective transport energy. For example, transport may occur by hopping between localized states that are exponentially distributed in energy which, as mentioned earlier, can give rise to an effective transport energy.[43] Alternatively, the low $E_c - E_{F,redox}$ may be the energy of an impurity band formed by intercalation of H^+ and Li^+ ions, or some weighted average of conduction band and impurity band energies.[48,49] We should also remark that if ${}_nE_F$ is within 90 meV of the conduction band edge at the highest V_{oc}, then the DOS there cannot be on the order of 8×10^{20} cm^{-3}, as expected if the effective electron mass (m_e^*) is ~10 times the bare electron mass (m_e),[50] because this would require an electron density ~9.4 times greater than actually present in the cell. Almost exactly the same observation has been made by other authors for DSCs based on the I_3^-/I^- electrolyte.[51] However, our data would be consistent with an effective conduction band DOS (N_c) of $\leq 8.5 \times 10^{19}$ cm^{-3} at 298 K, which would require that $m_e^* \approx 2.3m_e$. If this were the case, then a free electron mobility of 10^{-4} cm^2 V^{-1} s^{-1} can be calculated from $R_{t,0}$ (using eq S2 in the Supporting Information). This is at least 2 orders of magnitude smaller than values obtained from microwave and terahertz conductivity measurements,[52] which also indicates that the electron transport probed by IS does not predominantly occur via the conduction band.

For Y123-Co, an identical estimate for $E_c - E_{F,redox}$ of 0.74 eV is obtained at 298 K, increasing confidence in the analysis. However, T_c values derived from the slopes of the plots decrease with increasing temperature, which is not predicted by eq 11 (Figure S10). In order to confirm whether the above estimate of $E_c - E_{F,redox}$ for Y123-Co is reasonable, we have performed an alternative analysis using R_t–V_{oc} data and the measured temperature dependence of $E_{F,redox}$, which should be unaffected by the temperature dependence of T_c (Supporting Information). This analysis yields $E_c - E_{F,redox}$ = 0.75 and 0.79 eV for Z907-Co and Y123-Co, respectively. These values are slightly larger than those obtained from analysis of R_t–C_{meas} data, but close enough that they do not significantly alter our conclusions about the likely transport mechanism.

The data in Figure 3b also seem to indicate that, for the highest few C_{meas} values, ${}_nE_F$ actually reaches the transport energy. For such high ${}_nE_F$ eq 10 is unlikely to be valid, even if for no other reason than the breakdown of Boltzmann statistics, and thus "ideal" transport should not necessarily be expected. However, for data a few k_BT below the transport level, eq 10 may still be valid if electron–electron interactions can be neglected. Observation of ${}_nE_F$ approaching the transport level so closely has interesting consequences for the interpretation of impedance spectra recorded at high V_{oc}. Many authors, including ourselves, have asserted that R_t data obtained from impedance spectra where there is substantial overlap between transport and cathode time constants are unreliable.[21,24,26,44,45,53] However, these assertions are based, in part, on the belief that semi-log R_t–V_{oc} plots should remain linear indefinitely, which clearly cannot be the case on the basis of estimates of $E_c - E_{F,redox}$ found here and in previous works.[7,51] Recall that estimation of $R_{t,0}$ here does not rely on any of the R_t data obtained at high V_{oc} (it was not included in the global fit), so this cannot be the reason for the low estimates of $E_c - E_{F,redox}$. One must then *expect* some curvature of R_t–V_{oc} plots when V_{oc} becomes close to $E_c - E_{F,redox}$ due to, at least, the breakdown of Boltzmann statistics. Motivated by this realization, we have carefully analyzed the regression statistics from fits to impedance data using several variants of commonly employed equivalent circuit models, to investigate the circumstances under which R_t can and cannot be accurately determined (Supporting Information; also see ref 54 for a more general error analysis of DSC impedance data).[54] To briefly summarize, in the majority of cases we can find no reasonable statistical grounds for treating the R_t data as invalid or unreliable.

Now that we have an estimate of $E_c - E_{F,redox}$, and thus about the likely range of validity of eq 10, we are in a position to analyze the R_t–V_{oc} data in more detail. Whenever eq 10 is valid, it is possible to empirically estimate the extent of any energy level unpinning directly from the R_t–V_{oc} data, without requiring specific information about the electrical double layer at the TiO_2–solution interface. It is simple to show using eq 10 that the change in ϕ_s relative to some arbitrary reference condition, $\Delta\phi_{rel}$, is given by

$$\Delta\phi_{rel} = (V_{oc,ref} - V_{oc}) + \frac{k_BT}{q}\ln\left(\frac{R_{t,ref}}{R_t}\right) \quad (12)$$

where $V_{oc,ref}$ is an arbitrary reference photovoltage and $R_{t,ref}$ is the corresponding transport resistance. Here, we take $V_{oc,ref}$ as the lowest measured V_{oc}, which corresponds to the highest measured R_t. If the TiO_2 energy levels are fully pinned at $V_{oc,ref}$, then $\Delta\phi_{rel}$ is simply equal to $\Delta\phi_s$.

Figure 4a,b shows plots of changes in stored charge, ΔQ, versus $-\Delta\phi_{rel}$ for Z907-Co and Y123-Co. Here, ΔQ is defined

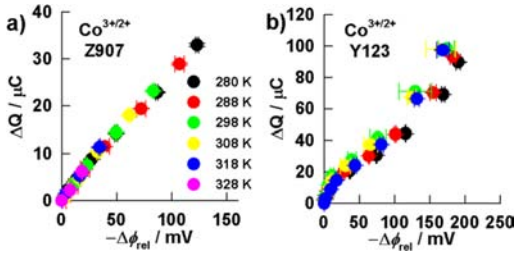

Figure 4. Correlation between changes in stored charge (ΔQ) and apparent changes in the TiO_2 electric potential ($\Delta\phi_{rel}$; estimated from R_t–V_{oc} data using eq 12) at various temperatures for DSCs employing $[Co(bpy)_3]^{3+/2+}$ as redox mediator and either Z907 (a) or Y123 (b) as sensitizer.

as the excess charge relative to the charge stored at the same $V_{oc,ref}$ used to calculate $\Delta\phi_{rel}$. The charge was estimated by numerical integration of C_{meas}–V_{oc} data and in principle is equal to the excess electronic charge stored in the TiO_2, which to ensure overall electroneutrality must equal the sum of the counter charge stored in the electrolyte, specifically adsorbed at the interface, and possibly intercalated into the TiO_2 lattice. Interestingly, a linear relationship is found between ΔQ and $-\Delta\phi_{rel}$ below ~50 mV for Z907-Co. The plots are also practically independent of temperature over the entire range. A correlation is also found for Y123-Co, but the plots are not linear.

The implication of the linear correlation between ΔQ and $-\Delta\phi_{rel}$ for Z907-Co is that the simplest possible model for the electrostatic capacitance (C_ϕ), consisting of a single, voltage- and temperature-independent capacitance, can *quantitatively* explain the non-ideality in the R_t–V_{oc} plots (note that the vast majority of the data are concentrated between 0 and −50 mV in Figure 4a). The slight deviation from linearity at higher $-\Delta\phi_{rel}$ may arise if ${}_nE_F$ approaches the transport energy too closely so that eq 10, and therefore eq 12, becomes invalid. It is also quite possible that the interfacial capacitance is potential-dependent, as is often found even in far simpler systems (e.g., a bare metal electrode).[55] The slope of the plot in Figure 4a corresponds to a microscopic areal capacitance of ~1.2 μF cm^{-2}. As mentioned by Natarajan and co-workers,[56] values in the range 1–3 μF cm^{-2} for the Helmholtz capacitance (C_H) at semiconductor surfaces have been derived using intensity-modulated photocurrent spectroscopy,[57−59] but we are not aware of similar data for dye-coated TiO_2 surfaces. Cappel and co-workers previously estimated C_H for a dye-sensitized TiO_2 electrode to be 4 or 6 μF cm^{-2}, depending on the dye used.[60] These values are of the same order as those obtained here and in our previous work (2.3–9.3 μF cm^{-2}),[26] and thus energy level unpinning seems to be a reasonable explanation for the non-ideality in the R_t–V_{oc} plots. The evidence for unpinning for Y123-Co is weaker due to the apparent proximity of ${}_nE_F$ to the transport energy at high V_{oc} (thus reducing the accuracy of eq 12); however, some degree of unpinning cannot be ruled out on the basis of these data.

If the non-ideality in R_t–V_{oc} data is caused by unpinning of the TiO_2 energy levels, it is necessary to reevaluate the C_{meas}–V_{oc} plots (Figure 1a–c). As we have shown previously,[26] C_{meas}–

dx.doi.org/10.1021/ja311743m | J. Am. Chem. Soc. 2013, 135, 3939–3952

V_{oc} data can be fitted to obtain C_ϕ and the TiO_2 DOS parameters if it is assumed that the underlying DOS is perfectly exponential and that C_ϕ is a constant. Doing so yields $C_\phi \approx 2$ μF cm^{-2} (microscopic area) for Z907-Co and $C_\phi \approx 4$ μF cm^{-2} for Y123-Co at 280 K (not shown). These values are close to, but slightly larger than, the values that can be derived directly from plots of ΔQ versus $\Delta\phi_{rel}$ (Figure 4); the discrepancy may arise if the DOS is not perfectly exponential or if there is some contribution to C_μ from the conduction band capacitance at high V_{oc}. In further support of the energy level unpinning explanation, charge/light-induced changes in interfacial electric fields at dye-sensitized TiO_2–solution interfaces, identified by Stark shifts in dye absorption spectra, have recently been reported.[60−62] However, we should also note that recent calculations indicate that oxidized dye molecules can induce a much larger Stark shift in the absorption spectra of adjacent dye molecules than TiO_2 electrons can.[63] With this in mind, it is important to remember that spectral shifts consistent with a Stark effect were also observed solely by biasing dye-sensitized electrodes *in the dark* to potentials where no oxidized dye molecules were present. Further evidence for substantial energy level unpinning was found in very recent variable-temperature spectroelectrochemistry experiments by Ondersma and Hamann.[64] Using unsensitized TiO_2 electrodes in a 0.2 M $LiClO_4$ acetonitrile solution, these authors found apparent conduction band shifts of up to 175 meV, very similar to the shifts found here (Figure 4a,b).

3.4. Modeling Recombination of TiO_2 Electrons with $Co[(bpy)_3]^{3+}$ Ions: Theoretical Basis. In this section we model recombination in these DSCs, considering both pinned and partially unpinned energy levels. We only focus on modeling R_{rec} since the other popular measure of recombination, the effective electron lifetime, $\tau_n = R_{rec}C_{meas}$,[65,66] is simply related to R_{rec} via C_{meas} and thus provides no additional information about recombination, aside from that already contained in the C_{meas}–V_{oc} data. Besides R_{rec} and τ_n, the steady-state V_{oc}–I_0 characteristics also contain information about recombination.[67−69] However, it turns out that this information is also mostly redundant because the V_{oc}–I_0 characteristics can be accurately predicted from the R_{rec}–V_{oc} characteristics and the carrier photogeneration efficiency (Figure S5).

The starting point for modeling R_{rec} is the definition

$$R_{rec} = \frac{1}{q^2 A}\left(\frac{dJ_{rec}}{d_n E_F}\right)^{-1} \tag{13}$$

where J_{rec} is the recombination flux. To obtain expressions for R_{rec} we first need to express J_{rec} in terms of ${}_nE_F$. For this we use a Gerischer-type charge-transfer model with Fermi–Dirac statistics for electrons in the TiO_2 (assuming all electrons share a common ${}_nE_F$)[70,71] and an energy-dependent rate constant so that, neglecting electron transfer from the electrolyte to the TiO_2, the recombination flux (through a unit projected electrode area) is given by

$$J_{rec} = rc_{ox}\int_{E_{F,redox}}^{\infty} f(E, {}_nE_F)g(E)k_{ET}(E)\,dE \tag{14}$$

where r is the electrode roughness factor, c_{ox} is the concentration of electron acceptors, $f(E,{}_nE_F)$ is the Fermi function, $g(E)$ is the density of electronic states in the TiO_2 and $k_{ET}(E)$ is the rate constant for charge transfer. Here, $k_{ET}(E)$ is taken to have units of cm^4 s^{-1} to facilitate comparison with rate constants measured at planar semiconductor electrodes.[72−74] This necessitates the inclusion of r to convert from flux through the microscopic electrode area to flux through the projected electrode area. This approach is only strictly valid for a planar electrode with $r = 1$ due to the three-dimensional nature of the electron-transfer problem which arises otherwise. This issue has recently been treated by Liu and Chen, who conclude that for spherical electrodes, a size dependence of the rate constant should only be observable for radii <5 nm,[75] suggesting that eq 14 should be a good approximation for the 10 nm radius particles used here. In other recent work the volume fraction of TiO_2 close enough to the interface to allow recombination was introduced into the rate equation to account for the electrode geometry.[66] We do not adopt this approach here because we believe it oversimplifies the problem; for example, the volume fraction of solution into which electron transfer occurs is not considered. We also find that electron lifetimes calculated using the expression given in ref 66 have dimensions of seconds per centimeter, instead of just seconds as expected.

$k_{ET}(E)$ is either taken as being independent of energy or calculated using either Marcus theory or a Butler–Volmer-type expression. For $k_{ET}(E)$ given by Marcus theory we use the relation

$$k_{ET}(E) = k_{ET,max}\exp\left(-\frac{(E - E_{F,redox} - \lambda)^2}{4\lambda k_B T}\right) \tag{15}$$

where $k_{ET,max}$ is the rate constant for activationless charge transfer and λ is the reorganization energy. For Butler–Volmer kinetics we use

$$k_{ET}(E) = k_{ET,0}\exp\left(\frac{\alpha_{BV}(E - E_{F,redox})}{k_B T}\right) \tag{16}$$

where $k_{ET,0}$ is the equilibrium rate constant and α_{BV} is the transfer coefficient.

When recombination only occurs via the conduction band, eq 14 can be replaced with

$$J_{rec,cb} = rc_{ox}n_c k_{ET}(E_c - \Delta\phi_s) \tag{17}$$

where n_c is the electron density at the conduction band edge and is given by

$$n_c = N_c\exp\left(\frac{({}_nE_F - E_c + \Delta\phi_s)}{k_B T}\right) \tag{18}$$

As before, $\Delta\phi_s$ accounts for any energy level unpinning and, if needed, can be estimated from experimental data using eq 12. It is worth noting that in this model the "conduction band" could refer to any other distribution of states, provided that they are sufficiently far above ${}_nE_F$ that their occupancy is governed by Boltzmann statistics.

When recombination occurs via band gap states, the full form of eq 14 must be used to obtain an expression for J_{rec}. We consider two possibilities for the band gap state distribution. In the first model, we assume that the DOS involved in recombination is proportional to C_{meas} according to eq 1. This relation is based on the assumption that the TiO_2 energy levels are always pinned, so that the only contribution to C_{meas} is C_μ. In the second model, we consider a perfectly exponential distribution of band gap states given by eq 3. Here, we do not quantitatively treat the case where the surface states involved in recombination have an entirely different distribution than that

dx.doi.org/10.1021/ja311743m | J. Am. Chem. Soc. 2013, 135, 3939−3952

inferred from $C_{meas}(V_{oc})$. This is because it is not possible to separate the contributions of the two types of state to the capacitance, so we have no independent means of inferring their distribution. To account for possible energy level unpinning, E_c is simply replaced by $E_c - \Delta\phi_s$, as in eqs 9, 10, 17, and 18. Using eqs 13−18, we have derived expressions for R_{rec} considering pinned or partially unpinned TiO_2 energy levels, with charge transfer occurring via the conduction band or via band gap states (Supporting Information).

3.5. Modeling Recombination in DSCs Employing the Y123 Dye and the Co[(bpy)$_3$]$^{3+/2+}$ Redox Mediator. Figure 5a shows the R_{rec}−V_{oc} characteristics for Y123-Co at temperatures ranging from 280 to 328 K. As also found for the R_t−V_{oc} data, the plots are only weakly dependent on temperature and almost overlap at higher voltages. However, this should not be interpreted as evidence for temperature-independent recombination kinetics because the voltage scale has not been corrected for the temperature dependence of $E_{F,redox}$ (Figure 1d). Furthermore, the slopes at low V_{oc} do decrease with increasing temperature as expected for conduction-band-mediated recombination with pinned energy levels, for which a slope of $-q/(2.303k_BT)$ decades per volt is predicted. However, at higher V_{oc} the slopes of the plots become shallower, deviating strongly from ideality and thus demanding a different explanation. Interestingly, the deviation from ideality begins to occur at the same V_{oc} as it does in R_t−V_{oc} plots, suggesting a common cause. Since R_{rec} and R_t can be determined practically independently of one another from impedance spectra (their effects are manifest in different frequency regimes), the shared features in both data sets can be viewed as further evidence of the validity of the R_t data. As already mentioned, the validity of the R_{rec} data itself is supported by good agreement with steady-state V_{oc}−I_0 data (Figure S5).

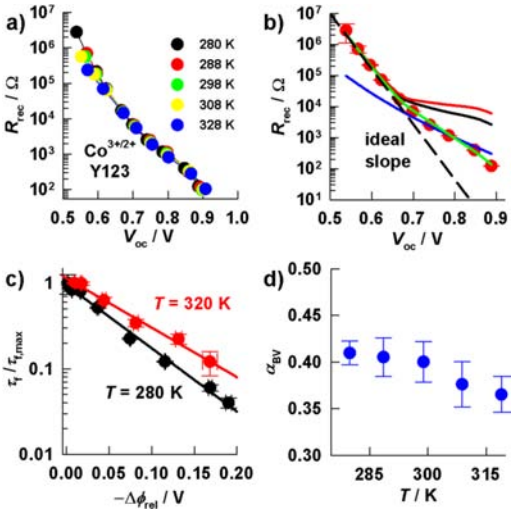

Figure 5. (a) Dependence of recombination resistance (R_{rec}) on photovoltage (V_{oc}) for a DSC employing $[Co(bpy)_3]^{3+/2+}$ as redox mediator and Y123 as sensitizer at various temperatures. (b) R_{rec}−V_{oc} characteristics at 280 K and a simulation of R_{rec} for recombination mediated by band gap states, assuming the density of band gap states is proportional to the measured capacitance, C_{meas}, and the rate constant is given by Marcus theory with λ = 1.4 eV (blue line, eq S10). Also shown are simulations for recombination via the conduction band with partially unpinned TiO_2 energy levels and an energy-independent rate constant (red line, eq S18), or an energy-dependent rate constant given either by Marcus theory (black line, eq S19) or by Butler−Volmer kinetics (green line, eq S20). (c) Dependence of the free electron lifetime ($\tau_f = R_{rec}/R_t$) on the apparent change of electric potential in the TiO_2 ($\Delta\phi_{rel}$) for the same DSC. (d) Dependence of Butler−Volmer transfer coefficient (α_{BV}) on temperature, derived from exponential fits to $\tau_f/\tau_{f,0}$−$\Delta\phi_{rel}$ plots.

Figure 5b shows the R_{rec}−V_{oc} characteristics at only 280 K, alongside various simulations based on the recombination models described above. The ideal slope of the plot at low V_{oc} is consistent with pinned energy levels and recombination occurring only via the conduction band. The ideal slope is *inconsistent* with significant recombination occurring via band gap states near $_nE_F$. Above ∼0.65 V the slope of the plot deviates from ideality, forcing us to abandon the simple picture of pinned energy levels and electron transfer via the conduction band at these voltages.

We find that it is *not* possible to model the data assuming recombination via band gap states that are distributed according to the C_{meas}−V_{oc} data (eq 1) with fully pinned energy levels. As an example, the blue line in Figure 5b shows a simulation for $g(E) \propto C_{meas}$ with k_{ET} given by Marcus theory (eq 15) taking λ = 1.4 eV, a value based on the inner-sphere reorganization energy of $[Co(bpy)_3]^{3+/2+}$ (∼1 eV) and a calculation of the outer-sphere contribution (∼0.4 eV) appropriate for an unsensitized TiO_2−acetonitrile interface.[66,74] The only adjustable parameter in the simulation was the maximal rate constant, $k_{ET,max}$, which was adjusted to obtain the best possible overlap with the data at high V_{oc}. Acceptable fits still cannot be obtained for *any* value of λ (which may be affected by the presence of the dye),[76,77] using Butler−Volmer kinetics (eq 16), or using an energy-independent k_{ET} (Figure S6). It is also worth noting that we cannot model the data by assuming recombination occurs via a perfectly exponential distribution of band gap states, with or without pinned energy levels, or assuming parallel recombination from band gap states and the conduction band. This is essentially because in all of these models, the ideal slope at low V_{oc} is not predicted.

We find that we *can* accurately model the R_{rec}−V_{oc} data if it is assumed that recombination occurs only via the conduction band and the non-ideality above 0.65 V arises from unpinning of the TiO_2 energy levels, as was also suggested to explain the R_t data. The red line in Figure 5b shows a simulation for conduction-band-mediated recombination and an energy-independent k_{ET}, with the amount of unpinning ($\Delta\phi_s$) estimated from R_t−V_{oc} data using eq 12 assuming $\Delta\phi_{rel} = \Delta\phi_s$. In this simulation, $E_c - E_{F,redox}$ was set to 1 eV on the basis of literature reports for a similar electrolyte composition[64,78] and N_c was set to 8×10^{20} cm^{-3} (note that for all models considered here the shape of R_{rec}−V_{oc} plots is independent of the value chosen for N_c). R_{rec} is overestimated by this simulation at high V_{oc}, indicating that an energy-independent k_{ET} is not realistic. This is not surprising as it is expected that k_{ET} will increase as the TiO_2 energy levels shift upward relative to the redox level and the driving force for recombination increases. The black line in Figure 5b shows a simulation using Marcus theory (eq 15) to quantify the change in k_{ET} as the energy levels unpin (i.e., setting $E = E_c - q\Delta\phi_s$ in eq 15), again with λ = 1.4 eV. Agreement between simulation and experiment is improved compared with an energy-independent k_{ET}, but for this value of λ, R_{rec} is still overestimated at high V_{oc}. The value of $k_{ET,max}$ used in this simulation (which, for the assumed $E_c - E_{F,redox}$ and N_c, fits the data at low V_{oc} very well) is ∼10^{-23} cm^4 s^{-1}, some 10^6−10^7 times smaller than the values found and predicted for unsensitized semiconductor electrodes.[66,72−74]

dx.doi.org/10.1021/ja311743m | J. Am. Chem. Soc. 2013, 135, 3939−3952

Even considering the uncertainty in $E_c - E_{F,redox}$ and N_c, the very large reduction in rate constant may indicate that the presence of the dye monolayer attenuates electronic coupling between TiO_2 donor states and $[Co(bpy)_3]^{3+}$ acceptor states. This possibility will be discussed in more detail later, in the light of the results obtained for Z907-Co.

It is possible to fit the Y123-Co R_{rec} data very well over the entire voltage range using Marcus theory to calculate k_{ET}, but unrealistic values of some or all of λ, $E_c - E_{F,redox}$, and $k_{ET,max}$ are required (not shown). For example, $\lambda \approx 6$ eV is required if $E_c - E_{F,redox} = 1$ eV, while $\lambda \approx 4$ eV is needed if $E_c - E_{F,redox} = 0.74$ eV, which is the minimum possible value for $E_c - E_{F,redox}$ based on the analysis of transport data mentioned previously, and in both of these cases unphysically large values of $k_{ET,max}$ are required. An excellent fit to the data over the entire voltage range can also be obtained using the Butler–Volmer expression (eq 16) to calculate k_{ET}, using transfer coefficient $\alpha_{BV} = 0.41$ (green line in Figure 5b). Note that here the transfer coefficient relates the conduction band recombination rate constant to the amount of band shift ($\Delta\phi_s$), *not* the current/resistance to the cell voltage ($_nE_F - E_{F,redox}$), as was the case in previous work.[31] It is not surprising that Butler–Volmer kinetics can also fit the data since, over a limited range of E, the Marcus expression can be approximated by the Butler–Volmer expression with a transfer coefficient given by

$$\alpha_{BV,Marcus} = k_B T \frac{d\log(k_{ET})}{d(E - E_{F,redox})} = \frac{\lambda - (E - E_{F,redox})}{2\lambda} \quad (19)$$

which for $\lambda = 1.4$ eV and $E - E_{F,redox} = 1$ eV yields $\alpha_{BV,Marcus} = 0.14$, much smaller than the experimental value of $\alpha_{BV} = 0.41$. It is possible that the surprisingly large values of λ or α_{BV} needed to fit the data over the entire voltage range arise from overestimation of $\Delta\phi_s$ by eq 12. Alternatively, the fact that better fits are obtained with the Butler–Volmer equation could reflect something more fundamental about the electron-transfer mechanism. Regardless of the precise explanation, it is clear that the R_{rec} data at low V_{oc} (<0.65 V) can only be explained by conduction-band (i.e., states far above $_nE_F$)-mediated transfer, which implies conduction-band-mediated transfer must also dominate at higher V_{oc} (unless a sudden increase in the density of band gap states occurs, which is not supported by the C_{meas}–V_{oc} data). It then follows that the deviation from ideality above 0.65 V is consistent with some degree of band unpinning and a concomitant increase in k_{ET}.

An alternative way of analyzing the R_{rec} data (which leads to identical conclusions) is to examine the dependence of the "free electron lifetime", τ_f, on $\Delta\phi_{rel}$. Bisquert and co-workers have pointed out that $\tau_f \propto R_{rec}/R_t$ if the free electron mobility is a constant.[65] For conduction-band-mediated electron transfer, τ_f is simply the inverse of $c_{ox}k_{ET}r/L$, and thus τ_f is expected to depend exponentially on $\Delta\phi_{rel}$ if Butler–Volmer kinetics are obeyed. Figure 5c shows semi-log plots of τ_f normalized to its maximum value, $\tau_{f,0}$, versus $\Delta\phi_{rel}$ and, for clarity, only data for the extremes of the temperature range are shown. As predicted, the plots are linear and their slopes become less steep with increasing temperature. Figure 5d shows that the transfer coefficient derived from the slopes, α_{BV}, depends quite weakly on T. Interpretation of this temperature dependence is difficult because the physical meaning of α_{BV} in this system is not clear at present, although in general it is expected to be determined by the symmetry of the energy barrier.[55] For this same reason, and because of complications arising from the temperature dependence of $E_{F,redox}$, a more detailed interpretation of the temperature dependence of τ_f or R_{rec} at a given V_{oc} will not be given here.

3.6. Modeling Recombination in DSCs Employing the Z907 Dye and the Co[(bpy)$_3$]$^{3+/2+}$ Redox Mediator. Figure 6a shows the R_{rec}–V_{oc} characteristics for Z907-Co at temperatures in the range 280–320 K. In contrast to the Y123-Co data, plots for Z907-Co are strongly temperature-dependent and exhibit highly non-ideal slopes over the entire V_{oc} range. The non-ideality is even observed at low V_{oc} where the R_t–V_{oc} plots were found to be almost ideal, ruling out the possibility that band unpinning is the sole cause for non-ideal recombination when the Z907 dye is used. Because of this, it can immediately be concluded that charge transfer mediated by band gap states must play at least some role in the recombination process for this cell. It is also noteworthy that at any given V_{oc} and T, R_{rec} for Z907 is 10–100 times smaller than that for Y123, which is a major reason for the inferior performance of Z907 under 1 Sun illumination (Figure S1).

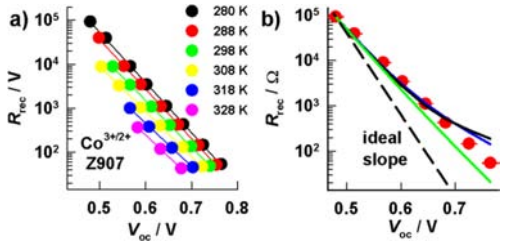

Figure 6. (a) Dependence of recombination resistance (R_{rec}) on photovoltage (V_{oc}) for a DSC employing $[Co(bpy)_3]^{3+/2+}$ as redox mediator and Z907 as sensitizer at various temperatures. (b) R_{rec}–V_{oc} characteristics at 280 K and simulations assuming recombination is mediated by band gap states either with a density proportional to the measured capacitance, C_{meas}, and pinned TiO_2 energy levels (blue line), with an exponential state distribution and pinned energy levels (green line) or with an exponential state distribution and unpinned energy levels (black line).

Figure 6b shows the R_{rec}–V_{oc} characteristics at only 280 K, together with various simulations based on plausible recombination mechanisms. For clarity, each simulation has been normalized to the highest experimental R_{rec} value. This does not affect the shape of the plots and can also be achieved by adjusting $k_{ET,max}$. The blue line shows a simulation for $g(E) \propto C_{meas}$, pinned energy levels, and k_{ET} given by Marcus theory (eq 15), again taking $\lambda = 1.4$ eV. The solid black line shows a simulation for recombination via a perfectly exponential distribution of states with partially unpinned energy levels. The extent of unpinning is estimated as before, T_c is obtained from C_{meas}–V_{oc} data at low V_{oc}, and k_{ET} is again given by Marcus theory with the same λ. The green line shows a simulation for recombination via the same exponential distribution of states, but with fully pinned energy levels.

It is obvious that none of the simulations in Figure 6b agree with the data well over the entire voltage range, but all predict approximately the correct deviation from ideality. Similar results are obtained for λ as low as 1 eV (corresponding to only inner-sphere reorganization) and for λ up to several eV larger (not shown). We interpret this as evidence that recombination occurs via an approximately exponential distribution of states that are distributed in energy in a similar way to the states giving rise to C_{meas}. However, as none of the

dx.doi.org/10.1021/ja311743m | J. Am. Chem. Soc. 2013, 135, 3939–3952

simulations fit the data to within experimental error, it is difficult to decide which the best recombination model is. The fit could be improved by assuming pinned energy levels and choosing an appropriate value for the band gap state distribution temperature, T_c, that is slightly different from that inferred from $C_{meas}-V_{oc}$ data. However, even if a different T_c is accepted (perhaps associated with a surface state distribution different to the bulk state distribution), a separate explanation for the non-ideal R_t-V_{oc} plots would still be required. Alternatively, the data could be explained by allowing the extent of energy level unpinning to be a little less than that estimated from R_t-V_{oc} plots (perhaps due to eq 12 becoming invalid when ${}_nE_F$ is near the transport energy), or by allowing a small amount of recombination to occur via the conduction band at high V_{oc}. Despite the obvious ambiguity here, a few important conclusions can still be drawn: (i) a large fraction of recombination must occur via band gap states in order to produce the non-ideal slope at low V_{oc}, (ii) the energetic distribution of these states is similar to that inferred from $C_{meas}-V_{oc}$ data, and (iii) the recombination data do not definitively *rule out* some energy level unpinning, and therefore this remains a plausible explanation for the non-ideality in the transport data, as discussed previously.

3.7. Influence of the Dye on Charge Recombination Mechanism. R_{rec} for Y123-Co is 10−100 times larger than that for Z907-Co at any given temperature or V_{oc}, as illustrated by Figure 7a for T = 298 K. This is the main reason that Y123-Co

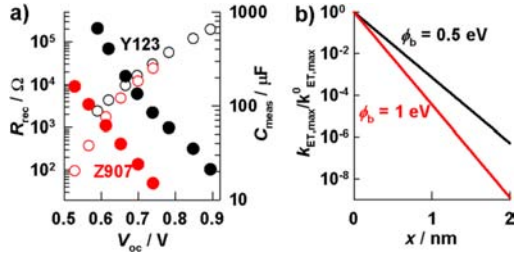

Figure 7. (a) Dependence of recombination resistance (R_{rec}, filled circles, left vertical axis) and measured capacitance (C_{meas}, open circles, right vertical axis) on photovoltage (V_{oc}) for DSCs employing $[Co(bpy)_3]^{3+/2+}$ as redox mediator and either Z907 (red) or Y123 (black) as sensitizer at 298 K. (b) Distance dependence of the tunneling probability for rectangular potential barriers with barrier heights of 0.5 and 1 eV.

exhibits higher V_{oc} and overall PCE under simulated solar irradiance. Results of the analysis in the previous section provide strong evidence that recombination occurs predominantly via the conduction band for Y123-Co, but via band gap states for Z907-Co. This conclusion can be drawn on the basis of data obtained at low V_{oc} and does not rely on our suggestion that the energy levels unpin at higher V_{oc} being correct. Since R_{rec} can be considered as a parallel combination of resistances for conduction band recombination ($R_{rec,cb}$) and band gap state recombination ($R_{rec,t}$), to cause a change in the slope of $\log(R_{rec})-V_{oc}$ from ideal (conduction band recombination) to non-ideal (band gap state recombination) *and* an overall decrease in total R_{rec}, it is necessary for $R_{rec,t}$ to decrease more than $R_{rec,cb}$ at any particular V_{oc} when changing dye from Y123 to Z907. The slope change alone could be produced by just increasing $R_{rec,cb}$, but this would not lead to the overall decrease in R_{rec}.

One of the most obvious possible causes for a decrease in $R_{rec,t}$ at a given V_{oc} is an increase in the density of band gap states near ${}_nE_F$. All other things being equal, a difference in the DOS near ${}_nE_F$ of *at least* 10−100 times would be required to reproduce the difference in R_{rec} between the two dyes. This could occur either due to the creation of new states by Z907 (or, equivalently, less efficient removal of states compared with Y123) or due to a downward shift in the TiO_2 energy levels with respect to the redox level. However, these possibilities can be ruled out on the basis of the slightly *lower* C_{meas} for Z907-Co compared to Y123-Co at any given V_{oc} (Figure 7a).

With differences in the energies and densities of TiO_2 donor states ruled out as being the cause for the change in recombination mechanism induced by changing dye, only two possibilities remain: either the acceptor state distribution, or the coupling between donor and acceptor states, depends on the nature of the dye. In the framework of Marcus−Gerischer theory, a change in acceptor state distribution implies a change of the reorganization energy. In principle, reducing the reorganization energy from the expected value of ∼1.4 eV to a value closer to the energy of the TiO_2 band gap states could induce a transition from conduction band to band gap state mediated recombination.[69] We have explored this possibility by simulating $R_{rec}-V_{oc}$ characteristics considering simultaneous recombination from the conduction band and band gap states, neglecting band unpinning and with k_{ET} given by Marcus theory. For $E_c - E_{F,redox}$ = 1 eV, T_c = 700 K and a density of band gap states chosen such that $R_{rec,t}$ is *just* negligible when λ = 1.4 eV ($R_{rec,t} \geq 10R_{rec,cb}$ over the experimental voltage range) a full transition to recombination via band gap states ($R_{rec,cb} \geq 10R_{rec,t}$) does not occur even for λ < 1 eV (Figure S7). Since the dye is probably not directly involved in the charge transfer, it is not reasonable to expect that the nature of the dye will affect λ so strongly, especially considering that inner-sphere reorganization makes up ∼1 eV of the expected 1.4 eV reorganization energy for $[Co(bpy)_3]^{3+/2+}$.[66,74]

A more reasonable explanation for the drop in R_{rec} is that the nature of the dye alters the strength of the electronic coupling between TiO_2 states and $[Co(bpy)_3]^{3+}$ acceptor states. This could arise due to some or all of the following: differences in the steric bulk of the dye affecting the distance between $[Co(bpy)_3]^{3+}$ ions and the TiO_2 surface,[10,28] differences in the ability of different dye mediums to attenuate the electronic coupling (i.e., different barrier heights), differences in the coverage/compactness of the dye monolayers, or differences in the ability of the dyes to bind $[Co(bpy)_3]^{3+}$ ions near the TiO_2 surface by Coulombic attraction.[14,16,77] However, for any of these explanations to be correct, electronic coupling with band gap states must be attenuated more than with conduction band states on changing from Z907 to Y123, otherwise the change in predominant recombination route would not be observed when changing dye. A possible mechanism for this involves the energy and distance dependence of the coupling. It is known that the electronic coupling decays approximately exponentially with distance so that, if the distance dependence of the reorganization energy is neglected,[64,66] $k_{ET,max}$ can be expressed as

$$k_{ET,max} = k^0_{ET,max} \exp[-\beta(x - x_0)] \quad (20)$$

where x is the distance from the electrode surface, x_0 is the distance of closest approach of redox species for an unsensitized electrode, $k_{ET,max,0}$ is the rate constant at $x = x_0$, and β is a decay

dx.doi.org/10.1021/ja311743m | J. Am. Chem. Soc. 2013, 135, 3939−3952

constant, typically of the order of 0.1−1 $Å^{-1}$ for molecular layers (dependent on bond conjugation).[79,80] If the dye monolayer is compact and pinhole-free, $[Co(bpy)_3]^{3+}$ ions will not be able to directly approach the TiO_2 surface, and $x - x_0$ will take the value of the dye layer thickness. The effect of Coulombic attraction between $[Co(bpy)_3]^{3+}$ ions and negatively charged dye molecules,[14,16,77] pinholes in the dye layer, etc. can still be accounted for within the framework of this model by defining an appropriately weighted effective approach distance and barrier height. For the simplest case of a rectangular-shaped barrier, β is given by

$$\beta = \frac{2}{\hbar}\sqrt{2m_e\phi_b} \tag{21}$$

where $\hbar$ is the reduced Planck's constant, m_e is the electron mass, and ϕ_b is the barrier height. To a rough first approximation, ϕ_b is the energy difference between the initial state in the TiO_2 (e.g., the conduction band edge) and the nearest available state on the dye (e.g., the LUMO).[81]

Figure 7b shows how changing the barrier height alters the distance dependence of $k_{ET,max}$. Two reasonable barrier heights have been chosen: the lower barrier (ϕ_b = 0.5 eV, β = 0.72 $Å^{-1}$) could represent an electron in the conduction band with the dye LUMO lying 0.5 eV above it, while the higher barrier (ϕ_b = 1 eV, β = 1.0 $Å^{-1}$) could represent an electron in a surface state 0.5 eV below the conduction band and thus 1 eV below the dye LUMO. We should stress that a rectangular barrier is almost certainly an oversimplification and the barrier heights used in this model may not have direct physical significance. However, the chosen barrier heights produce β values that fall within the range of observed values for molecular layers and will therefore suffice for the purposes of illustration. It is clear from Figure 7b that the rate constant drops off more quickly with distance for larger barrier heights (i.e., lower lying TiO_2 states) and that differences in dye layer thickness of the order of 1 nm and differences in barrier height of the order of 0.5 eV are sufficient to induce a 10−100-fold change in rate constant. It follows that if Y123 and Z907 are assumed to possess similar energy barriers but the bulkier Y123 dye presents a wider barrier than the Z907 dye (this seems likely on the basis of the optimized geometries for these dyes),[82,83] the relative amount of band-gap-mediated recombination compared to conduction band recombination will be lower for Y123 than for Z907. This explanation is also applicable if the more negatively charged Z907 dye binds $[Co(bpy)_3]^{3+}$ ions more strongly than the Y123 dye;[77] in this case, the average charge-transfer distance is also expected to be reduced, again increasing the relative importance of band gap states in the recombination process for a given barrier height.

4. CONCLUSIONS

Efficient DSCs employing $[Co(bpy)_3]^{3+/2+}$ as redox mediator and either organic dye Y123 or ruthenium dye Z907 as sensitizer were characterized using impedance spectroscopy over a range of temperatures and photovoltages. A transmission line model was used to extract the TiO_2 capacitance and the transport and recombination resistances. Capacitance−photovoltage plots shifted toward higher photovoltage with increasing temperature due to a negative shift in the electrolyte redox Fermi energy, which was estimated to have a temperature coefficient of −1.62 meV K^{-1}. The capacitance−photovoltage plots were not exponential over the entire voltage range, and the nature of the dye and electrolyte solution changed the slopes/shapes of the plots. This could be caused either by a non-exponential TiO_2 DOS that depends on the dye and electrolyte composition, or by varying degrees of unpinning of the TiO_2 energy levels, or both.

The temperature dependence of transport resistance and capacitance data was used to determine an effective electron-transport energy that was 0.74 eV above the redox Fermi energy, substantially lower than expected for the TiO_2 conduction band, indicating that transport may occur by another mechanism such as hopping via localized states. The dependence of transport resistance on photovoltage was generally found to be non-ideal, with ideality increasing as photovoltage was decreased. For cells employing the Z907 dye, capacitance, transport, and photovoltage data are quantitatively consistent with an explanation of non-ideality involving partial unpinning of the semiconductor energy levels due to charging of an almost constant Helmholtz capacitance. Interpretation of transport data is more complicated for cells employing the Y123 dye because the quasi-Fermi energy appears to reach the transport energy at very high photovoltage.

The dependence of recombination resistance on photovoltage and temperature for DSCs employing the Y123 dye is consistent with a model where recombination only occurs via the conduction band (or other states far above the quasi-Fermi energy), the TiO_2 energy levels are partially unpinned, and the electron-transfer rate constant obeys Butler−Volmer-like kinetics with a transfer coefficient in the range 0.35−0.41. No convincing evidence for band gap state mediated recombination was found for the Y123 dye.

In contrast to Y123, when the Z907 dye is used recombination clearly occurs via band gap states near the quasi-Fermi energy. Because of this, the recombination resistance for Z907 cells is 1−2 orders of magnitude smaller than for Y123 cells at any given photovoltage or temperature. This leads to lower 1 Sun photovoltage, fill factor, and efficiency for cells employing Z907. The reason for the change in recombination mechanism brought about by changing the dye is thought to be that the two dyes differ in their ability to attenuate electronic coupling between $Co[(bpy)_3]^{3+}$ and states in the TiO_2, probably due to differences in the steric bulk of the dyes. Because band gap states exist at lower energies than conduction band states, the applicable tunneling barrier height is expected to be larger for band gap states and thus the rate constant is predicted to be more sensitive to the electron-transfer distance. Consequently, recombination from band gap states is expected to be suppressed more effectively than from higher lying conduction band states when increasing the size of the dye. Alternative explanations involving changes in the density of TiO_2 band gap states or their energetic matching with $[Co(bpy)_3]^{3+}$ acceptor states were ruled out by extensive simulations of recombination.

■ ASSOCIATED CONTENT

Supporting Information

Current−voltage characteristics of the DSCs used in this study. Equivalent circuit used to fit impedance spectra. Temperature dependence of the electron-transport resistance pre-factor ($R_{t,0}$) for the case of conduction band transport. Reliability and validity of R_t at high V_{oc}. Correspondence between V_{oc}−I_0 and R_{rec}−V_{oc} characteristics. Derivation of expressions for R_{rec}. Additional R_{rec} simulations illustrating the effect of varying λ. Stability of DSCs during impedance measurements. Predicted dependence of R_t on ${}_nE_F$. "Ideality" of R_t−V_{oc} data. Dependence of T_c on temperature and alternative estimation of $E_c - E_{F,redox}$.

dx.doi.org/10.1021/ja311743m | J. Am. Chem. Soc. 2013, 135, 3939−3952

This material is available free of charge via the Internet at http://pubs.acs.org.

AUTHOR INFORMATION

Corresponding Author

qing.wang@nus.edu.sg

Author Contributions

‡Y.L. and J.R.J. contributed equally.

Notes

The authors declare no competing financial interest.

ACKNOWLEDGMENTS

This work was financially supported by URC grant No. R-284-000-075-112 and NRF CRP grant No. R-284-000-079-592. We thank Dr. Chenyi Yi for providing the Y123 dye and Dr. Xingzhu Wang for synthesizing the $[Co(bpy)_3]^{3+/2+}$ complexes.

REFERENCES

(1) Grätzel, M. *Acc. Chem. Res.* **2009**, *42*, 1788.
(2) Yella, A.; Lee, H.-W.; Tsao, H. N.; Yi, C.; Chandiran, A. K.; Nazeeruddin, M. K.; Diau, E. W.-G.; Yeh, C.-Y.; Zakeeruddin, S. M.; Grätzel, M. *Science* **2011**, *334*, 629.
(3) Oregan, B.; Grätzel, M. *Nature* **1991**, *353*, 737.
(4) Watson, D. F.; Meyer, G. J. *Annu. Rev. Phys. Chem.* **2005**, *56*, 119.
(5) Listorti, A.; O'Regan, B.; Durrant, J. R. *Chem. Mater.* **2011**, *23*, 3381.
(6) Peter, L. *Acc. Chem. Res.* **2009**, *42*, 1839.
(7) Bisquert, J. *J. Phys. Chem. C* **2007**, *111*, 17163.
(8) Boschloo, G.; Hagfeldt, A. *Acc. Chem. Res.* **2009**, *42*, 1819.
(9) Tian, H. N.; Jiang, X. A.; Yu, Z.; Kloo, L.; Hagfeldt, A.; Sun, L. C. *Angew. Chem., Int. Ed.* **2010**, *49*, 7328.
(10) Feldt, S. M.; Gibson, E. A.; Gabrielsson, E.; Sun, L.; Boschloo, G.; Hagfeldt, A. *J. Am. Chem. Soc.* **2010**, *132*, 16714.
(11) Wang, M. K.; Chamberland, N.; Breau, L.; Moser, J. E.; Humphry-Baker, R.; Marsan, B.; Zakeeruddin, S. M.; Grätzel, M. *Nat. Chem.* **2010**, *2*, 385.
(12) Li, D. M.; Li, H.; Luo, Y. H.; Li, K. X.; Meng, Q. B.; Armand, M.; Chen, L. Q. *Adv. Funct. Mater.* **2010**, *20*, 3358.
(13) Liu, Y.; Jennings, J. R.; Parameswaran, M.; Wang, Q. *Energy Environ. Sci.* **2011**, *4*, 564.
(14) Nusbaumer, H.; Moser, J. E.; Zakeeruddin, S. M.; Nazeeruddin, M. K.; Grätzel, M. *J. Phys. Chem. B* **2001**, *105*, 10461.
(15) Sapp, S. A.; Elliott, C. M.; Contado, C.; Caramori, S.; Bignozzi, C. A. *J. Am. Chem. Soc.* **2002**, *124*, 11215.
(16) Nusbaumer, H.; Zakeeruddin, S. M.; Moser, J. E.; Grätzel, M. *Chem.—Eur. J.* **2003**, *9*, 3756.
(17) Cameron, P. J.; Peter, L. M.; Zakeeruddin, S. M.; Grätzel, M. *Coord. Chem. Rev.* **2004**, *248*, 1447.
(18) Nakade, S.; Makimoto, Y.; Kubo, W.; Kitamura, T.; Wada, Y.; Yanagida, S. *J. Phys. Chem. B* **2005**, *109*, 3488.
(19) Nelson, J. J.; Amick, T. J.; Elliott, C. M. *J. Phys. Chem. C* **2008**, *112*, 18255.
(20) Klahr, B. M.; Hamann, T. W. *J. Phys. Chem. C* **2009**, *113*, 14040.
(21) Ondersma, J. W.; Hamann, T. W. *J. Phys. Chem. C* **2009**, *114*, 638.
(22) Liberatore, M.; Petrocco, A.; Caprioli, F.; La Mesa, C.; Decker, F.; Bignozzi, C. A. *Electrochim. Acta* **2010**, *55*, 4025.
(23) DeVries, M. J.; Pellin, M. J.; Hupp, J. T. *Langmuir* **2010**, *26*, 9082.
(24) Wang, H.; Nicholson, P. G.; Peter, L.; Zakeeruddin, S. M.; Grätzel, M. *J. Phys. Chem. C* **2010**, *114*, 14300.
(25) Tsao, H. N.; Yi, C.; Moehl, T.; Yum, J.-H.; Zakeeruddin, S. M.; Nazeeruddin, M. K.; Grätzel, M. *Chemsuschem* **2011**, *4*, 591.
(26) Jennings, J. R.; Liu, Y.; Wang, Q. *J. Phys. Chem. C* **2011**, *115*, 15109.
(27) Cameron, P. J.; Peter, L. M. *J. Phys. Chem. B* **2003**, *107*, 14394.
(28) Liu, Y. R.; Jennings, J. R.; Huang, Y.; Wang, Q.; Zakeeruddin, S. M.; Grätzel, M. *J. Phys. Chem. C* **2011**, *115*, 18847.
(29) Fabregat-Santiago, F.; Garcia-Belmonte, G.; Mora-Sero, I.; Bisquert, J. *Phys. Chem. Chem. Phys.* **2011**, *13*, 9083.
(30) Bisquert, J. *Phys. Chem. Chem. Phys.* **2008**, *10*, 49.
(31) Wang, Q.; Ito, S.; Grätzel, M.; Fabregat-Santiago, F.; Mora-Seró, I.; Bisquert, J.; Bessho, T.; Imai, H. *J. Phys. Chem. B* **2006**, *110*, 25210.
(32) Gritzner, G.; Lewandowski, A. *J. Chem. Soc., Faraday Trans.* **1991**, *87*, 2599.
(33) Benko, J.; Vollarova, O. G.; Gritzner, G. *Phys. Chem. Chem. Phys.* **2001**, *3*, 1471.
(34) Kopidakis, N.; Neale, N. R.; Zhu, K.; Lagemaat, J. v. d.; Frank, A. J. *Appl. Phys. Lett.* **2005**, *87*, 202106.
(35) Zhu, K.; Kopidakis, N.; Neale, N. R.; van de Lagemaat, J.; Frank, A. J. *J. Phys. Chem. B* **2006**, *110*, 25174.
(36) O'Regan, B. C.; Durrant, J. R. *Acc. Chem. Res.* **2009**, *42*, 1799.
(37) Bard, A. J.; Bocarsly, A. B.; Fan, F. R. F.; Walton, E. G.; Wrighton, M. S. *J. Am. Chem. Soc.* **1980**, *102*, 3671.
(38) Bisquert, J.; Zaban, A. *Appl. Phys. a—Mater. Sci. Process.* **2003**, *77*, 507.
(39) Fabregat-Santiago, F.; Mora-Seró, I.; Garcia-Belmonte, G.; Bisquert, J. *J. Phys. Chem. B* **2002**, *107*, 758.
(40) Lyon, L. A.; Hupp, J. T. *J. Phys. Chem.* **1995**, *99*, 15718.
(41) Bisquert, J. *J. Phys. Chem. B* **2002**, *106*, 325.
(42) Madelung, O. *Introduction to Solid-State Theory*; Springer-Verlag: Berlin, 1995.
(43) Gonzalez-Vazquez, J. P.; Anta, J. A.; Bisquert, J. *Phys. Chem. Chem. Phys.* **2009**, *11*, 10359.
(44) Zhu, K.; Jang, S.-R.; Frank, A. J. *J. Phys. Chem. Lett.* **2011**, *2*, 1070.
(45) Zhu, K.; Jang, S.-R.; Frank, A. J. *Energy Environ. Sci.* **2012**, *5*, 9492.
(46) Lobato, K.; Peter, L. M.; Wurfel, U. *J. Phys. Chem. B* **2006**, *110*, 16201.
(47) Lobato, K.; Peter, L. M. *J. Phys. Chem. B* **2006**, *110*, 21920.
(48) Wang, Q.; Zhang, Z.; Zakeeruddin, S. M.; Gratzel, M. *J. Phys. Chem. C* **2008**, *112*, 7084.
(49) Halverson, A. F.; Zhu, K.; Erslev, P. T.; Kim, J. Y.; Neale, N. R.; Frank, A. J. *Nano Lett.* **2012**, *12*, 2112.
(50) Enright, B.; Fitzmaurice, D. *J. Phys. Chem.* **1996**, *100*, 1027.
(51) O'Regan, B. C.; Durrant, J. R. *J. Phys. Chem. B* **2006**, *110*, 8544.
(52) Dunn, H. K.; Peter, L. M.; Bingham, S. J.; Maluta, E.; Walker, A. B. *J. Phys. Chem. C* **2012**, *116*, 22063.
(53) Jennings, J. R.; Liu, Y.; Safari-Alamuti, F.; Wang, Q. *J. Phys. Chem. C* **2011**, *116*, 1556.
(54) Jennings, J. R.; Wang, Q. *J. Electrochem. Soc.* **2012**, *159*, F141.
(55) Bard, A. J.; Faulkner, L. R. *Electrochemical Methods: Fundamentals and Applications*, 2nd ed.; Wiley: New York, 2001.
(56) Natarajan, A.; Oskam, G.; Searson, P. C. *J. Phys. Chem. B* **1998**, *102*, 7793.
(57) Oskam, G.; Schmidt, J. C.; Searson, P. C. *J. Electrochem. Soc.* **1996**, *143*, 2538.
(58) Schefold, J. *J. Electroanal. Chem.* **1992**, *341*, 111.
(59) de Wit, A. R.; Vanmaekelbergh, D.; Kelly, J. J. *J. Electrochem. Soc.* **1992**, *139*, 2508.
(60) Cappel, U. B.; Feldt, S. M.; Schöneboom, J.; Hagfeldt, A.; Boschloo, G. *J. Am. Chem. Soc.* **2010**, *132*, 9096.
(61) Ardo, S.; Sun, Y.; Staniszewski, A.; Castellano, F. N.; Meyer, G. J. *J. Am. Chem. Soc.* **2010**, *132*, 6696.
(62) Ardo, S.; Sun, Y.; Castellano, F. N.; Meyer, G. J. *J. Phys. Chem. B* **2010**, *114*, 14596.
(63) Pastore, M.; Angelis, F. D. *J. Phys. Chem. Lett.* **2011**, *2*, 1261.
(64) Ondersma, J. W.; Hamann, T. W. *Energy Environ. Sci.* **2012**, *5*, 9476.
(65) Bisquert, J.; Fabregat-Santiago, F.; Mora-Seró, I. N.; Garcia-Belmonte, G.; Giménez, S. *J. Phys. Chem. C* **2009**, *113*, 17278.
(66) Ondersma, J. W.; Hamann, T. W. *J. Am. Chem. Soc.* **2011**, *133*, 8264.

(67) Cameron, P. J.; Peter, L. M.; Hore, S. *J. Phys. Chem. B* **2005**, *109*, 930.
(68) Salvador, P.; Hidalgo, M. G.; Zaban, A.; Bisquert, J. *J. Phys. Chem. B* **2005**, *109*, 15915.
(69) Jennings, J. R.; Wang, Q. *J. Phys. Chem. C* **2010**, *114*, 1715.
(70) Bisquert, J.; Zaban, A.; Salvador, P. *J. Phys. Chem. B* **2002**, *106*, 8774.
(71) Mora-Seró, I.; Bisquert, J. *Nano Lett.* **2003**, *3*, 945.
(72) Royea, W. J.; Fajardo, A. M.; Lewis, N. S. *J. Phys. Chem. B* **1997**, *101*, 11152.
(73) Hamann, T. W.; Gstrein, F.; Brunschwig, B. S.; Lewis, N. S. *J. Am. Chem. Soc.* **2005**, *127*, 7815.
(74) Hamann, T. W.; Gstrein, F.; Brunschwig, B. S.; Lewis, N. S. *J. Am. Chem. Soc.* **2005**, *127*, 13949.
(75) Liu, Y.; Chen, S. *J. Phys. Chem. C* **2012**, *116*, 13594.
(76) Liu, Y.-P.; Newton, M. D. *J. Phys. Chem.* **1994**, *98*, 7162.
(77) Mosconi, E.; Yum, J.-H.; Kessler, F.; Gómez García, C. J.; Zuccaccia, C.; Cinti, A.; Nazeeruddin, M. K.; Grätzel, M.; De Angelis, F. *J. Am. Chem. Soc.* **2012**, *134*, 19438.
(78) Redmond, G.; Fitzmaurice, D. *J. Phys. Chem.* **1993**, *97*, 1426.
(79) Albinsson, B.; Mårtensson, J. *J. Photochem. Photobiol. C: Photochem. Rev.* **2008**, *9*, 138.
(80) Wold, D. J.; Haag, R.; Rampi, M. A.; Frisbie, C. D. *J. Phys. Chem. B* **2002**, *106*, 2813.
(81) Salomon, A.; Boecking, T.; Seitz, O.; Markus, T.; Amy, F.; Chan, C.; Zhao, W.; Cahen, D.; Kahn, A. *Adv. Mater.* **2007**, *19*, 445.
(82) Malapaka, C.; Ganugula, R.; Chikkam Srinivasa, R.; Thogiti, S.; Paidi Yella, R.; Jun-Ho, Y.; Mahammad Khaja, N.; Michael, G. *Adv. Nat. Sci.: Nanosci. Nanotechnol.* **2011**, *2*, 035016.
(83) Dualeh, A.; De Angelis, F.; Fantacci, S.; Moehl, T.; Yi, C.; Kessler, F.; Baranoff, E.; Nazeeruddin, M. K.; Grätzel, M. *J. Phys. Chem. C* **2011**, *116*, 1572.